

Comparative study of metallic and dielectric helix photonic metamaterial

Arvinder Singh Chadha,¹ Deyin Zhao,¹ and Weidong Zhou¹

¹Department of Electrical Engineering, University of Texas at Arlington, Arlington, TX 76019, USA

*wzhou@uta.edu

Abstract: We compare the performance of metallic and dielectric thin film helix photonic metamaterial numerically. The simulated metal helix provides a 4 μm broad band circular dichroism with a polarization suppression ratio of 20:1. The transmission efficiency of the metal helix drops significantly with increasing number of helix turns and angle of incidence. Contraire, the simulated silicon dielectric helix structure provides an extremely high polarization suppression ratio above 2,300:1 with almost 100% transmission over a wide range of incident angles. The results provided highlights the trade-offs between the transmission efficiency and the specular and angular bandwidth for designing practical thin-film circular polarizers.

©2014 Optical Society of America

OCIS codes: (160.1585) Chiral media; (160.3918) Metamaterials; (160.4670) Optical materials.

References and links

1. A. Saha, K. Bhattacharya, and A. K. Chakraborty, "Reconfigurable achromatic half-wave and quarter-wave retarder in near infrared using crystalline quartz plates," *Opt. Eng.* **50**(3), 034004 (2011).
2. G. De Filpo, F. P. Nicoletta, and G. Chidichimo, "Cholesteric emulsions for colored displays," *Adv. Mater.* **17**(9), 1150–1152 (2005).
3. S. Tibuleac and R. Magnusson, "Narrow-linewidth bandpass filters with diffractive thin-film layers," *Opt. Lett.* **26**(9), 584–586 (2001).
4. J. K. Gansel, M. Thiel, M. S. Rill, M. Decker, K. Bade, V. Saile, G. von Freymann, S. Linden, and M. Wegener, "Gold helix photonic metamaterial as broadband circular polarizer," *Science* **325**(5947), 1513–1515 (2009).
5. Z. Yang, M. Zhao, and P. Lu, "Similar structures, different characteristics: optical performances of circular polarizers with single-, double-, and multi-helical metamaterials," in *Proc. SPIE Vol.*, 2011, pp. 79331.
6. J. K. Gansel, M. Wegener, S. Burger, and S. Linden, "Gold helix photonic metamaterials: a numerical parameter study," *Opt. Express* **18**(2), 1059–1069 (2010).
7. Z. Y. Yang, M. Zhao, and P. X. Lu, "A numerical study on helix nanowire metamaterials as optical circular polarizers in the visible region," *Photonics Technology Letters, IEEE* **22**(17), 1303–1305 (2010).
8. J. Fischer and M. Wegener, "Three-dimensional direct laser writing inspired by stimulated-emission-depletion microscopy [Invited]," *Opt. Mater. Express* **1**(4), 614–624 (2011).
9. Y. K. Pang, J. Lee, H. Lee, W. Y. Tam, C. Chan, and P. Sheng, "Chiral microstructures (spirals) fabrication by holographic lithography," *Opt. Express* **13**(19), 7615–7620 (2005).
10. Y. J. Park, K. M. A. Sobahan, and C. K. Hwangbo, "Wideband circular polarization reflector fabricated by glancing angle deposition," *Opt. Express* **16**(8), 5186–5192 (2008).
11. N. Tétreault, G. von Freymann, M. Deubel, M. Hermatschweiler, F. Pérez-Willard, S. John, M. Wegener, and G. A. Ozin, "New route to three-dimensional photonic bandgap materials: silicon double inversion of polymer templates," *Adv. Mater.* **18**(4), 457–460 (2006).
12. K. Balasundaram, P. K. Mohseni, Y.-C. Shuai, D. Zhao, W. Zhou, and X. Li, "Photonic crystal membrane reflectors by magnetic field-guided metal-assisted chemical etching," *Appl. Phys. Lett.* **103**(21), 214103 (2013).
13. N. Yamada, T. Ijiri, E. Okamoto, K. Hayashi, and H. Masuda, "Characterization of antireflection moth-eye film on crystalline silicon photovoltaic module," *Opt. Express* **19**(S2 Suppl 2), A118–A125 (2011).
14. L. Li, "Use of Fourier series in the analysis of discontinuous periodic structures," *J. Opt. Soc. Am. A* **13**(9), 1870–1876 (1996).
15. X. Wang, W. Gao, J. Hung, and W. Y. Tam, "Optical activities of large-area SU8 microspirals fabricated by multibeam holographic lithography," *Appl. Opt.* **53**(11), 2425–2430 (2014).
16. J. Lee and C. Chan, "Polarization gaps in spiral photonic crystals," *Opt. Express* **13**(20), 8083–8088 (2005).
17. L. Li, "Multilayer modal method for diffraction gratings of arbitrary profile, depth, and permittivity," *J. Opt. Soc. Am. A* **10**(12), 2581–2591 (1993).

18. P. Vukusic and J. R. Sambles, "Photonic structures in biology," *Nature* **424**(6950), 852–855 (2003).
 19. M. G. Moharam and T. K. Gaylord, "Rigorous coupled-wave analysis of planar-grating diffraction," *J. Opt. Soc. Am.* **71**, 811–818 (1981).
 20. K. C. Johnson, "Coupled scalar wave diffraction theory," *Appl. Phys. (Berl.)* **24**(3), 249–260 (1981).
 21. E. D. Palik, *Handbook of Optical Constants of Solids: Index*, vol. 3 (Elsevier, 1998).
 22. S. Makarov, *Antenna and EM Modeling with MATLAB* (Wiley-Interscience, 2002).
 23. M. McCall, "Axial electromagnetic wave propagation in inhomogeneous dielectrics," *Math. Comput. Model.* **34**(12-13), 1483–1497 (2001).
 24. M. Thiel, M. Decker, M. Deubel, M. Wegener, S. Linden, and G. von Freymann, "Polarization stop bands in chiral polymeric three-dimensional photonic crystals," *Adv. Mater.* **19**(2), 207–210 (2007).
-

1. Introduction

Optical circular polarizers find their use in a variety of applications like displays, optical communication, photography, sensors and spectroscopy. A perfect circular polarizer should transmit one state of the circularly polarized light (CPL) and completely block the other CPL state. Wavelength range, acceptance angle, aperture size, mechanical stability, transmission efficiency and polarization suppression ratio are some of the key parameters that are considered when choosing a circular polarizer. Cholesteric liquid crystals (CLC) and a combination of linear polarizer with a quarter-wave plate are the two most commonly used methods to generate circularly polarized light [1, 2]. The bandwidth of a CLC film is determined by the liquid crystals birefringence (Δn) and the pitch length [3]. The performance of the LCs is further limited by their high viscosity and poor chemical and photo stabilities. The linear polarizer absorbs 50% of the incident light and the optical efficiency is halved. More recently metal helix structures have shown circular dichroism [4]. A lot of work is documented on the performance optimization and limitations on the optical performances of circular polarizers with metallic helical metamaterials [5–7]. Compared with the former two methods, the helical circular polarizer has advantages of broad frequency ranges, and compact structures which are convenient to integrating with other optical devices. However, the metal absorption leads to low transmission efficiency and poor polarization suppression ratio (PSR), which is defined as the ratio of the transmitted light intensity of one state of the circularly polarized light to the other state of the circularly polarized light. The loss associated with metallic metamaterials operating at optical frequencies presents a grand challenge in applications of optical functional metamaterials for integrated photonics applications.

One of the solutions to the low loss optical functional metamaterials is the use of all dielectric materials, which can be intrinsically zero-loss. The dielectric structures are more mechanically stable and feature the added advantage of higher temperature resistance, and damage threshold as compared to the metal helical polarizers. Methods like glancing angle deposition (GLAD), normal direct laser writing (DLW), stimulated-emission-depletion (STED) DLW and two template inversion methods hold promising future to fabricate high quality multi-turn dielectric helix circular polarizers [8–11]. For the fabrication of semiconductor based helix structures, recently demonstrated magnetic field guided metal-assisted chemical-etching (MacEtch) process can be a viable fabrication technique [12]. Complete three dimensional photonic band gaps have been reported by dielectric spiral photonic crystals, however, they did not exhibit circular dichroism [13–15]. A numerical study of dielectric helical structures comprising of hexagonal lattice exhibited polarization gaps with circular dichroism [16]. More recently circular dichroism using dielectric is demonstrated experimentally [17, 18]. However, the device performance is largely limited by the low index contrast between the photoresist and the background. So it is preferable to have semiconductor based dielectric structures for higher index contrast and integration with other passive/active devices for integrated optics on chip. In this paper we numerically investigate an all-dielectric circular polarizer consisting of silicon helix on glass substrate. We show that the simulated silicon dielectric helixes provides extremely high polarization suppression ratio above 2,300:1 with almost 100% transmission over a wide range of incident angles.

2. Simulation and design

2.1 Simulation methodology

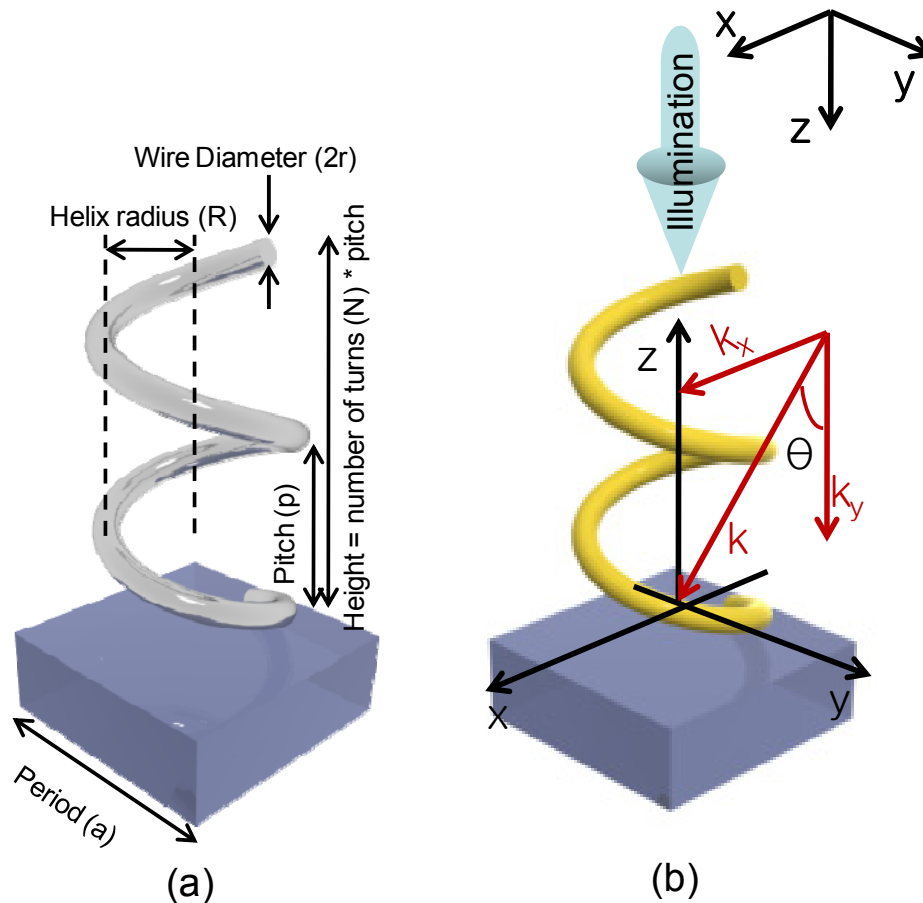


Fig. 1. Schematic diagram of (a) silicon dielectric helix and (b) gold metal helix photonic metamaterial on glass substrate. The helix comprises of square lattice with period (a), major radius (R), helix wire radius (r), pitch (p), number of turns (N) and incident angle (θ)

The rigorous coupled-wave analysis (RCWA) technique [19, 20] is employed to compute the transmission for left and right circularly polarized light. The entire structure is built using rectangular blocks with a staircase approximation. The Maxwell equations are rigorously calculated at each wavelength. The solution inside each layer is solved as a Fourier expansion. Boundary conditions are used to match the tangential electromagnetic field components. The electromagnetic modes are calculated in each layer and are propagated analytically through each layer. The fundamental and higher order forward and backward wave diffraction efficiencies are determined by solving the coupled wave equations for the transmitted and reflected waves. The electric field is the sum of a series of Fourier components based on the solutions from the coupled wave equations from which the total transmission and reflection waves are computed for the transverse electric (TE) and transverse magnetic (TM) fields. The solutions of the TE and TM waves are then translated to compute the response of the helix structure into the transmission and reflection of the right and left circularly polarized light. When the tip of the electric field vector of the incident plane wave, at a given point in space, describes a circle and traces a right hand (RH) helix as

time progresses, the plane wave is said to be RH polarized wave. Shown in Fig. 1 is the schematic of the unit cell of a dielectric silicon helix and a gold metal helix photonic metamaterial on glass substrate. The helices are arranged periodically in a square lattice. The dielectric helix period (a), major radius (R), axial pitch (p) and wire radius (r) are taken to be $1.5\ \mu\text{m}$, $0.550\ \mu\text{m}$, $2\ \mu\text{m}$ and $0.2\ \mu\text{m}$ respectively. The gold metal helix period, major radius, axial pitch and wire radius are taken to be $2\ \mu\text{m}$, $1\ \mu\text{m}$, $2\ \mu\text{m}$ and $0.2\ \mu\text{m}$ respectively. The refractive index of the glass substrate is assumed to be 1.45 for all simulations. The dielectric silicon helix assumes a non-dispersive refractive index of 3.48 as silicon is transparent at the wavelengths of interests here (from $1.5\ \mu\text{m}$ to $7\ \mu\text{m}$). The optical constants for the gold metal is taken from reference [21], which is optimized for large bandwidth operation. The parameters for the dielectric helix are also near optimal, based on the scan of all key parameters for broadband operation. The light is incident along the axis of the helix. Results are shown for right-handed helices. By symmetry, the RCP needs to be exchanged by LCP for left handed helices.

2.2 Comparison between metallic and dielectric helix photonic metamaterial

Shown in Fig. 2 is the evolution of circular dichroism from metallic and dielectric helices. Metallic helix with one pitch behaves like a split ring resonator characterized by sharp descreet resonances. The end-fire geometry of the metallic helix structure results in different transmission for the right and left circularly polarized light [22]. As the number of turns of the metallic helix increase, the resonance weakens and the on axis ratio increase. The response of the metal helices is dominated by the interaction of internal resonances and mutual coupling of the helix [4]. This mutual coupling of the helices is responsible for broadband nature, however, the transmission drops due to increased metal absorption. A circularly polarized light with wavelength equal to the pitch of the dielectric spiral is completely reflected due to Bragg reflection. This circular Bragg reflection due to uniaxial nonhomogeneous refractive index distribution along the propagation direction is responsible for the circular dichroism in the dielectric helix structure [23]. When the effective wavelength of the light inside the dielectric spiral matches the pitch of the helix along the propagation direction, there is maximum light matter interaction and the light field peaks inside the dielectric spiral for one polarization state [24]. Inside the polarization band the light decays exponentially for the other polarization state. In summary, there is a tradeoff between transmission efficiency and the bandwidth while implementing circular polarizers for practical applications.

The width of the polarization stop band is determined by the index contrast and the number of the turns (Fig. 3). For a given pitch height, when the number of turns increase the width of the polarization stop band increase and then saturates. Increasing the number of helix turns further has negligible effects on the transmission spectrum near the Bragg region. Only three turns are needed to increase the PSR by a factor of hundred over a broad bandwidth of $500\ \text{nm}$. The metal helix structure with 3 turns, the unwanted metal absorption limits its transmission efficiency around 60%.

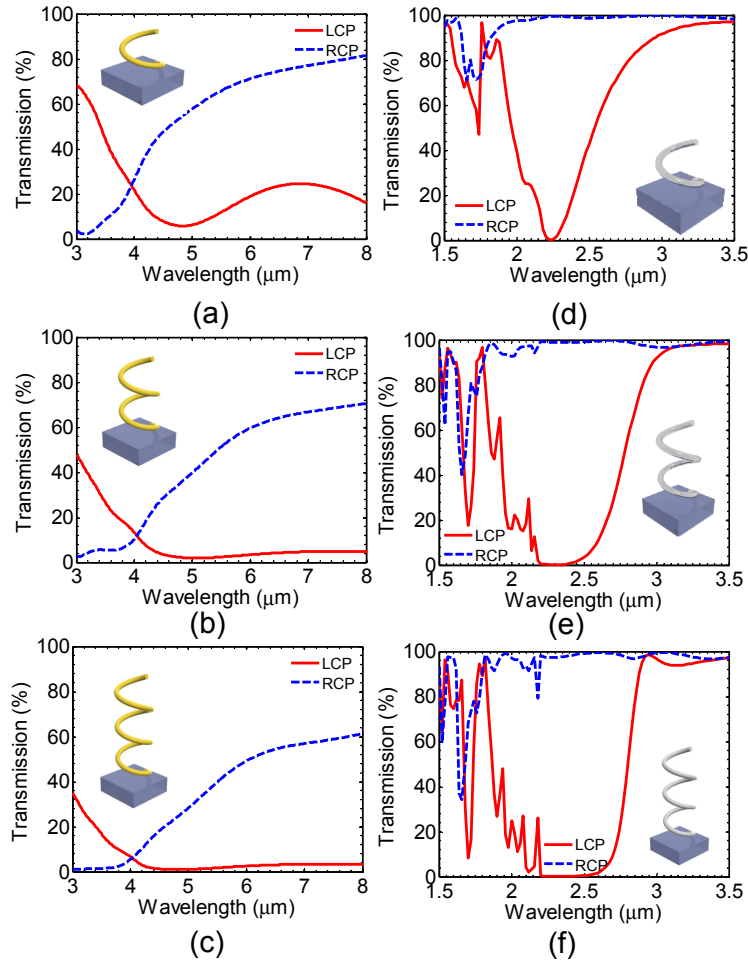


Fig. 2. Simulated transmission for the left circularly polarized light and the right circularly polarized light for 1 turn, 2 turns and 3 turns of the (a – c) gold metal and (d – f) silicon dielectric helix respectively. The inset shows the schematic of the simulated helix.

All the simulations so far have assumed the propagation of light along the helix axis. In practicality the incident light has certain angular spread. Shown in Fig. 4 is the simulated angular dependence of the metallic and dielectric helix metamaterial. At non-normal incidence, the produced polarization state seen by the helix structure becomes elliptical and a relatively large amount of light leaks through the helix. Hence the polarization suppression ratio falls with increasing angle of incidence (AOI). The gold metal helix is very susceptible to incident angular. Significantly deterioration is observed at a 10 degree deviation from surface normal [6]. The transmission falls below 30% and the polarization suppression ratio reduces to less than 10:1 for incident angles greater than 30 degrees for the metal helixes. The dielectric helix maintains greater than 80% transmission efficiency at oblique incidences with relatively high polarization suppression ratios. At oblique incidence, the effective index increases as seen by the circularly polarized light resulting in a redshift of the dichroic band. The dielectric silicon helix provides large angular tolerance with high transmission efficiency at the expense of reduced dichroic bandwidth.

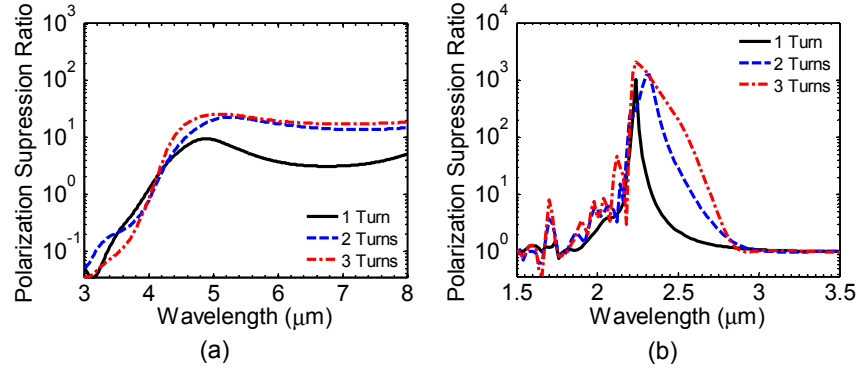


Fig. 3. Simulated polarization suppression ratio in semi log scale for the (a) gold metal and (b) silicon dielectric helix photonic metamaterial.

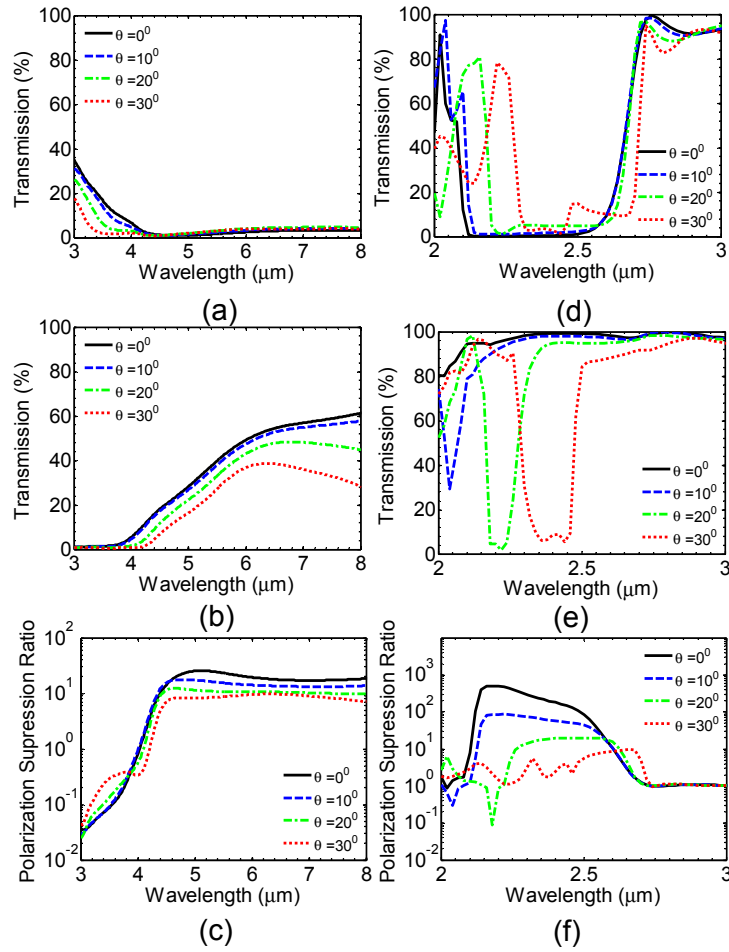


Fig. 4. Simulated transmission for the left circularly polarized light, right circularly polarized light and polarization suppression ratio for various incident angles for (a – c) the gold metal and (d – f) silicon dielectric helix photonic metamaterial.

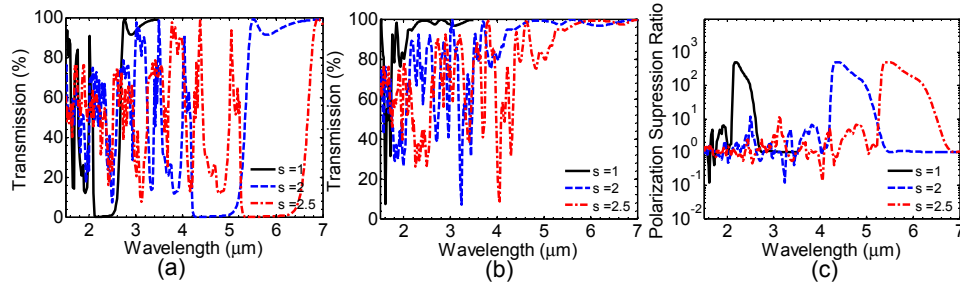


Fig. 5. Simulated transmission for (a) the left circularly polarized light, (b) the right circularly polarized light, and (c) the polarization suppression ratio of the silicon dielectric helix photonic metamaterial.

The losses of the metal helix structures make them inferior to the dielectric helix structures in the infrared region. Scalability of the helixes allows the tuning of the polarization gaps while maintaining the polarization suppression ratio. The variable “s” in Fig. 5 is the scalability parameter. All the helix geometric parameters are scaled by a factor “s”. The dielectric helix period (a) and axial pitch (p) are taken to be $1.5\ \mu\text{m}$ and $1.8\ \mu\text{m}$ respectively. The helix major radius (R) and wire radius (r) are taken to be $0.367a$ and $0.1333a$ for all the scaled simulation. A broadband spectral tuning is easily achievable with a dielectric spiral while maintaining high suppression ratio and transmission efficiency. The bandwidth increases from about $0.5\ \mu\text{m}$ at around $2 - 3\ \mu\text{m}$ wavelength spectrum band to about $1.3\ \mu\text{m}$ at around $5 - 7\ \mu\text{m}$ wavelength spectrum band. As shown the performance comparison summary in Table 1, the relative bandwidth, defined as the ratio of the spectral bandwidth to the center wavelength, remains almost constant (21%), which is expected, similar to the well developed theory in dielectric photonic crystal structures. We expect similar performance with high transmission at oblique incidence for the scaled dielectric helixes and did not perform angular simulations. A judicious choice of dielectric helix parameters also allows the circular reflection band to be tuned to the visible spectrum to reflect red, green and blue light for high quality display applications.

Table 1. Performance comparison between silicon helix on glass and metal helix on glass.

	Silicon Helix on glass substrate (a = $1.5\ \mu\text{m}$, R = $0.55\ \mu\text{m}$, p = $1.8\ \mu\text{m}$ and r = $0.1333a$)			Metal helix on glass substrate (a = $2\ \mu\text{m}$, R = $1\ \mu\text{m}$, p = $2\ \mu\text{m}$ and r = $0.1\ a$)
Maximum Transmission (T)	~100%			~60%
Absorption (A)	A = 0%			A > 40%
Maximum Transmission Polarization suppression ratio (PSR _{TRANS})	500:1			17:1
Wavelength at max. PSR (λ_{max})	2.24 μm	4.32 μm	5.5 μm	7 μm
Specular Bandwidth (μm)	0.48	0.95	1.18	4.8
Wavelength Range (μm)	2.19 – 2.67	4.21 – 5.16	5.27 – 6.45	4.58 – 9.42
Relative bandwidth (%)	21.4	22	21.5	68.5
Helix scaling parameter (s)	S=1	S= 2	S= 2.5	-
Angular Bandwidth (ABW)	30° ABW	-	-	20° ABW
Transmission at max. angle	~85%	-	-	~50%

3. Conclusions

In summary, we have compared the optical properties of the numerically simulated metallic and dielectric helix photonic metamaterials. Only three turns metallic helix photonic metamaterial provide around 3 μm circular dichroism. However, the unwanted metal absorption limits the polarization suppression ratio to 20:1 and transmission efficiency to about 60%. Furthermore, the slight deviations from the surface normal illumination reduce the polarization suppression ratio to 10:1 and the transmission efficiency to below 40%. The lossless dielectric structures make them superior to the metal helixes in the infrared region. The numerically simulated silicon dielectric helixes can give almost 100% transmission efficiency and polarization suppression ratio exceeding 2000:1 independent of the spectral location. The simulated relative bandwidth remains almost unchanged to be around 21%. The dielectric helix polarizer provides transmission efficiency greater than 85% for one circularly polarized light is maintained for incident angles as high as 30°. These results highlight the design trade-offs between transmission efficiency and the specular and angular bandwidth while implementing circular polarizers for practical applications.

Acknowledgments

The work was partially supported by US ARO (W911NF-09-1-0505) and by US AFOSR MURI program (FA9550-08-1-0337).